applied sciences

MDPI

Article

Computational Modeling of U-Shaped Seismic Dampers for Structural Damage Mitigation

Víctor Tuninetti [1,*], Álvaro Gómez [2], Flavia Bustos [3], Angelo Oñate [4], Jorge Hinojosa [5], Calogero Gallo [6], Anne-Marie Habraken [6,7] and Laurent Duchêne [6]

1 Department of Mechanical Engineering, Universidad de La Frontera, Temuco 4811230, Chile
2 Master Program in Engineering Sciences, Faculty of Engineering, Universidad de La Frontera, Temuco 4811230, Chile; a.gomez07@ufromail.cl
3 Doctoral Program in Engineering Systems, Faculty of Engineering, University of Talca, Curicó 3340000, Chile; flavia.bustos@utalca.cl
4 Department of Materials Engineering (DIMAT), Faculty of Engineering, Universidad de Concepción, Concepción 4070415, Chile; aonates@udec.cl
5 Department of Industrial Technologies, University of Talca, Curicó 3340000, Chile; jhinojosa@utalca.cl
6 Department ArGEnCo-MSM, University of Liège, 4000 Liège, Belgium; cgallo@uliege.be (C.G.); anne.habraken@uliege.be (A.-M.H.); l.duchene@uliege.be (L.D.)
7 F.R.S.—FNRS, Rue d'Egmont 5, 1000 Bruxelles, Belgium
* Correspondence: victor.tuninetti@ufrontera.cl

Abstract: U-shaped seismic dampers, passive metallic devices that dissipate energy by cyclic plastic deformation, are designed to mitigate the effects of seismic loads on structures. This study focuses on the development of an advanced computational model of a U-shaped damper, chosen for its unique design of variable thickness and width, which contributes to its superior performance. The simulation uses nonlinear finite element analysis and a bilinear hardening model calibrated to the actual stress–strain curve of the low-carbon steel. To ensure accuracy, a rigorous mesh convergence analysis is performed to quantify numerical prediction errors and establish a model suitable for predicting local deformation phenomena, including strain and stress fields, throughout the displacement-based loading protocol. Mesh sensitivity analysis, performed by examining the equivalent stress and cumulative plastic strain, derives the damper hysteresis curve and confirms the convergence criteria of the mesh within the experimentally observed plastic response range of the material. The resulting computational model is a novel contribution that provides reliable predictions of local inhomogeneous deformation and energy dissipation, essential for optimizing damper design and performance through more sophisticated damage-fatigue models that guarantee the lifetime of a damper.

Keywords: seismic dampers; seismic hazard mitigation; cumulative equivalent plastic strain; numerical modeling; engineering design

Citation: Tuninetti, V.; Gómez, Á.; Bustos, F.; Oñate, A.; Hinojosa, J.; Gallo, C.; Habraken, A.-M.; Duchêne, L. Computational Modeling of U-Shaped Seismic Dampers for Structural Damage Mitigation. *Appl. Sci.* **2024**, *14*, 10238. https://doi.org/10.3390/app142210238

Academic Editor: Dario De Domenico

Received: 7 October 2024
Revised: 4 November 2024
Accepted: 5 November 2024
Published: 7 November 2024

1. Introduction

Large earthquakes can result in significant human and financial losses, exemplified by the substantial damage caused by the two highest magnitude earthquakes in recent years: Chile, with USD 30 billion [1], and Japan, with USD 300 billion [2]. To mitigate such damage, anti-seismic devices such as passive, active, semiactive, and hybrid systems modify the response of a structure to seismic action by isolating, restraining, or dissipating energy [3–8]. Among these, passive dissipation systems offer lower costs compared to other types and are one of the most suitable for maintaining the integrity of structures under seismic loads [9]. For instance, metallic dampers that function under plastic deformation [10] present a variety of proposed geometries, such as plates [3,11], vertical bars [12], arch shapes [13], and U shapes [14–22].

U-shaped seismic dampers (USSDs) were first proposed in 1972 by J.M. Kelly et al. [14]. Subsequent enhancements to the original design have been introduced, such as the modification proposed by Mehdi Ebadi Jamkhaneh et al. [15], who proposed a USSD with both ends symmetrically closed, demonstrating that the thickness of the damper is a key geometric characteristic that improves its performance in terms of cycle number, deformation amplitude, and resistance loss percentage [15]. Moreover, Can-Xin Qiu et al. [16] introduced an adaptation that incorporates three ribs, which are different sizes and positioned perpendicular to the plate faces, with the aim of increasing the stiffness and strength of the damper. This modification significantly increased the stiffness, strength, and energy dissipation according to the rib size.

U-shaped seismic dampers are applied to the damping-isolation of buildings [23] under steel frames [24] or girders [25,26], and in bracings [27,28]. U-shaped dampers placed under components for base isolation could be integrated with rubber bearings and do not transmit vertical force [29]. These U-shaped dampers proposed as a simple base isolation control for medium-rise buildings have been reported to be installed in structures such as Isahaya City Hall and the Japanese Red Cross Ishinomaki Hospital [30]. In the case of lightweight structures, adaptive control of load-bearing structures manipulates internal stresses through actuators [31], thus requiring more complex components, and maintenance for functional safety and reliability, as well as energy consumption. With proper design, U-shaped seismic dampers show potential for passive seismic dissipation of lightweight structures.

Nippon Steel, a Japanese company specializing in global structural technology, commercially distributes a U-shaped damper that features increased thickness and a reduced width-to-length ratio. A study conducted by Diana Ene et al. [17] on this model concluded that it is highly unlikely to fracture during a single seismic event. Additionally, it has been established that the rate of change of the load is negligible for the damper.

Currently, several studies have explored different types of U-shaped steel dampers and proposed advanced methods to analyze their behavior under cyclic loading. Although simplified approaches, such as the use of weighted least-squares support vector machine algorithms, as suggested by Khatibinia et al. [18], can be effective in optimizing performance indices and proposing new damper models, they may not fully capture the complex localized behavior of these devices. Accurately assessing local stress, strain, and energy dissipation often requires the development of detailed analytical and numerical models [20–22]. U-shaped dampers, through numerical modeling, allow determining the effects of geometric parameters on the energy dissipation capacity and deformation capacity under cyclic loading. Detailed finite element analysis is crucial to capturing the complex behavior of U-shaped steel dampers. However, a significant research gap exists in ensuring adequate meshing strategies for reliable numerical modeling of USSDs. The complex geometries and localized deformation mechanisms inherent to these devices necessitate careful consideration of mesh density and element type to ensure solution accuracy and minimize computational cost [3,32,33]. Insufficient mesh refinement can lead to inaccurate stress and strain predictions, particularly in regions of high stress concentration, ultimately compromising the reliability of design optimizations based on these models. Therefore, reliable numerical models are needed to evaluate local stress, strain, and energy dissipation, providing a basis for design optimization. More detailed models that can thoroughly characterize local strain and stress are essential to develop high-performance U-shaped dampers for seismic applications and optimize their geometry to improve energy dissipation and performance.

This work presents the development of a computational model that reliably predicts the performance behavior of U-shaped metallic dampers through the integration of an elastoplastic model with rigorous mesh convergence analysis, enhancing the accuracy of predictions related to local deformation and energy dissipation capacity often overlooked in prior research. By addressing the local behavior, this approach lays the groundwork for more sophisticated models that consider damage prediction and fatigue behavior, ulti-

mately leading to safer designs for structural resilience during seismic events. Nonlinear finite element analysis is employed, with material characterization derived from the reported stress–strain curve of low-carbon steel. The sensitivity of the numerical results to mesh refinement is assessed across various loading protocols, ensuring the robustness of the applied method.

2. Materials and Methods

This section presents the method for material calibration of the bilinear hardening model of low-carbon JIS SM-490 steel. The computational simulation is also explained, including finite element analysis, software, elements, boundary conditions, and investigated loadings. The mesh convergence method based on Richardson extrapolation is also described to assess the quality of the numerical results.

2.1. Model Selection

The key geometric parameters of the U-shaped metallic damper include the projected lengths of the straight and curved sections, the radius of the curved section, the width, and the thickness (Figure 1a,b). The damper operates by moving the upper and lower straight bolted clamped sections in opposing directions, transitioning from elastic deformation to plastic deformation under cyclic loading. The mode of deformation is bending dominated by two plastic hinges, which enables the dissipation of the structure's kinetic energy during a seismic event. Since Nippon Steel proposed several types of USSD, UD-40 (Figure 1a) was selected as the model for experimentation because of its smaller size than the other models. For example, the displacement until failure is lower than that of UD50 [19]. The UD-40 damper differs from the other dampers mainly in its geometrical characteristics, with a greater thickness and both lower and variable widths (Figure 1b).

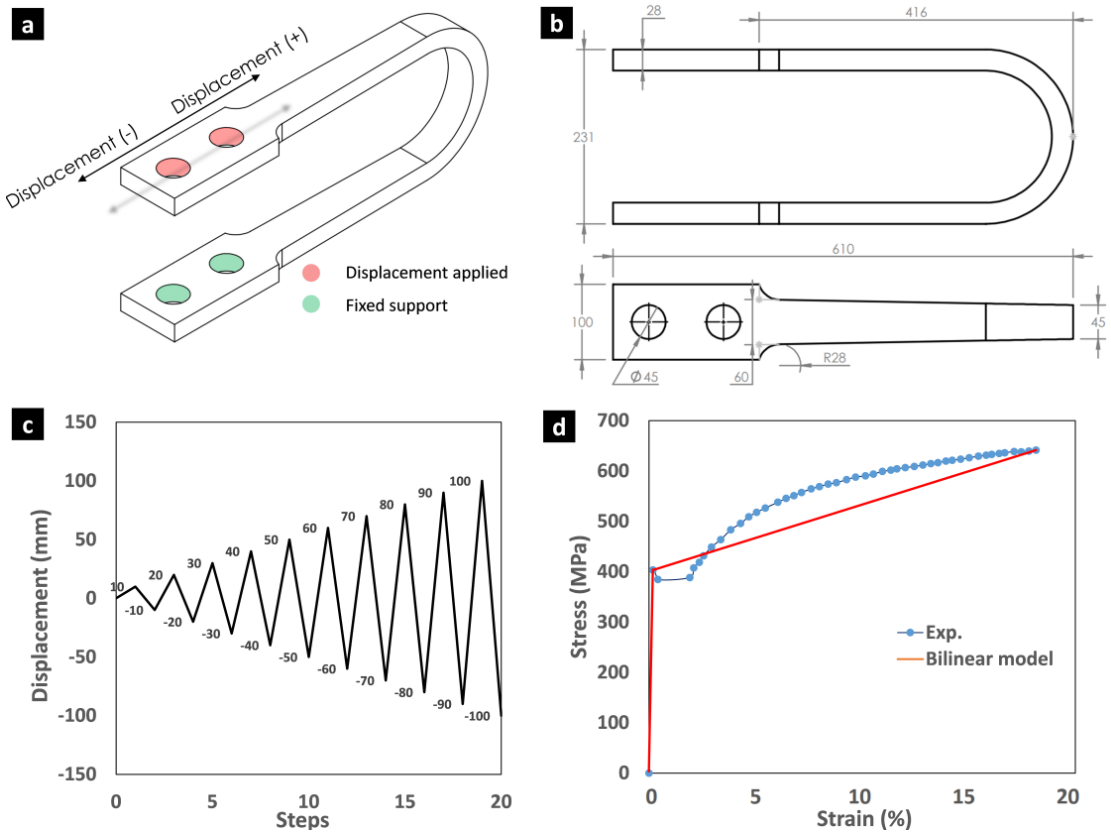

Figure 1. (**a**) UD-40 model with boundary conditions applied. (**b**) Upper and front sight of UD-40 USSD with dimensions in mm. (**c**) Load protocol applied to the damper. (**d**) True stress–strain curve from experimental data reported for JIS-SM490 fitted with the bilinear hardening model.

2.2. Material Calibration

The material selected according to the Nippon Steel technical report is JIS-SM490 structural steel [19]. The mechanical behavior of structural steel reported by Liu Y. [23] in the form of an engineering stress–strain curve, obtained from tensile tests of flat bar specimens, is transformed to true stress–strain definitions using Equations (1) and (2) [34].

$$\varepsilon_{true} = ln(1 + \varepsilon_{eng}) \quad (1)$$

$$\sigma_{true} = \sigma_{eng}(1 + \varepsilon_{true}) \quad (2)$$

where ε_{true}, ε_{eng}, σ_{true}, and σ_{eng} are the true strain, engineering strain, actual stress, and engineering stress, respectively.

The resulting elastoplastic stress–strain curve used in this work for material model characterization is shown by blue dotted line (Figure 1d). Then, bilinear hardening is applied to the material model, where the plasticity section of the stress–strain curve is approximated as linear behavior from the yield strength point to the ultimate tensile stress point as represented by the red line in Figure 1d. The slope of the plastic section line is the tangent modulus. Note that this bilinear model is underestimating the true stress, but this assumed error is in the safer size as suggested by Szybinski and Romanowicz [35]. Table 1 shows the material properties of the identified bilinear hardening model from the computed true stress–strain data.

Table 1. Material properties of JIS-SM490 for metallic damper simulations [23].

Yield Strength (MPa)	Ultimate Tensile Stress (MPa)	Young Modulus (GPa)	Tangent Modulus (MPa)
403.3	641.4	215.8	1324.7

2.3. Boundary Conditions and Meshings

The complete damping system may be composed of multiple USSDs. However, the evaluation of the damper is considered embedded between a lower plate and an upper plate, which is fixed to the structure through bolts. Ansys Workbench 2022 R2 software is used for the simulations. As a boundary condition, the fixed support is applied on the lower bores of the damper, as shown in Figure 1a. The dimensions of the UD-40 model selected are given in Figure 1b. The loads are applied as remote displacement on one axis (Figure 1a) with a 10-cycle load protocol with a maximum displacement of 100 mm in both directions, starting at 10 mm and increasing by 10% per cycle (Figure 1c).

2.4. Mesh Convergence Criterion

To obtain a precise prediction of the result, mesh convergence is needed. This requires several simulations to analyze the results of the equivalent von Mises stress, equivalent plastic strain, and accumulated equivalent plastic strain (AEPS). Additionally, 3 different load protocols of 1, 5, and 10 cycles are selected to determine the effect of number of cycles on the numerical results of the dissipation device (Table 2).

Table 2. Three load protocols of 1, 5, and 10 cycles are applied for mesh convergence analysis.

Cycles	Displacement (mm)										
1	0	±100	–	–	–	–	–	–	–	–	
5	0	±20	±40	±60	±80	±100	–	–	–	–	
10	0	±10	±20	±30	±40	±50	±60	±70	±80	±90	±100

Convergence analysis of the results in terms of the mesh size is performed via Richardson extrapolation [36]. This method considers a high-order estimate of the continuum value at zero mesh size from a series of lower-order discrete values. Equations (3) to (5) are used to calculate the estimated fractional error, which is then compared with the sizes of the

elements. The mesh size of each model using hexahedral-dominant elements is shown in Figure 2. A homogeneous element density is selected for the analyzed models, meaning that if smaller or more numerous elements are required for the thickness, the element size is also reduced throughout the damper.

$$E_1 = \frac{\varepsilon}{r^p - 1} \tag{3}$$

where

$$\varepsilon = \frac{\sigma_2 - \sigma_1}{\sigma_1} \tag{4}$$

$$r = \frac{h_2}{h_1} \tag{5}$$

In this case, ε represents the relative error given by Equation (4), where σ_2 and σ_1 are the maximum equivalent stresses of the 4.8 mm size element vs. the maximum equivalent stress of each mesh size model. Furthermore, r is the grid refinement ratio; then, h_2 and h_1 are the two grids, where h_1 represents the finest one. Finally, p is the grade of the method. Equation (6) seeks the minimum error through the results given from the grids h_2 and h_1. The result of these equations gives the convergence point [36]. When a second order is assumed (the error is reduced quadratically), the minimum error $f_{h=0}$ is given by:

$$f_{h=0} \cong \frac{f_1 - f_2}{r^2 - 1} \tag{6}$$

To understand the behavior of the device against different quantities of load steps in a static structural study, the mesh convergence for three different load protocols is used.

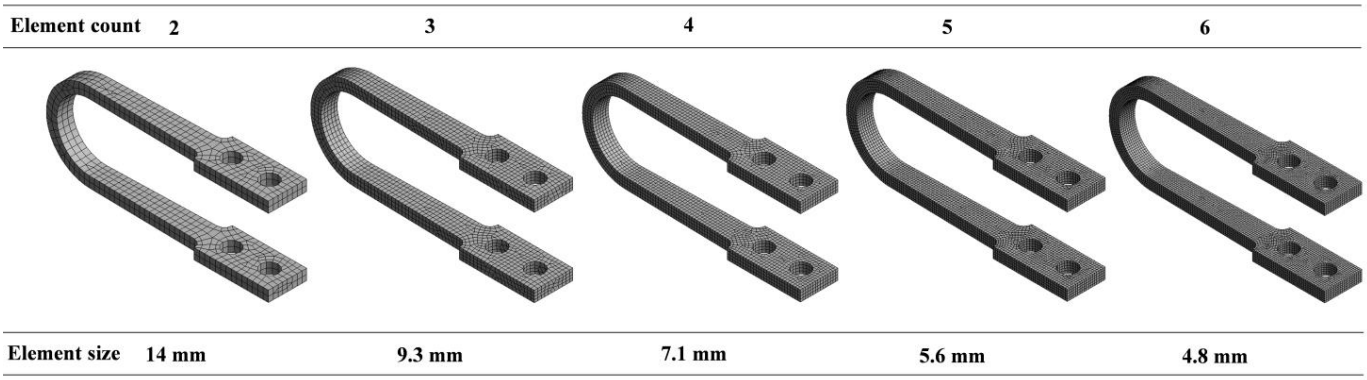

Figure 2. Finite element models of the U-shaped damper with increasing mesh density through the thickness.

2.5. Simulation Setting

To establish a realistic simulation, a large deflection was considered to capture significant deformations. Additionally, surface stress and nonlinear data options were activated to provide detailed information on these behaviors. For the boundary conditions, remote displacement was used to restrict undesired movements in directions different from the x-axis. Finally, a hex-dominant meshing method was used to obtain hexahedral elements. Compared with tetrahedral elements, hexahedral elements generally result in more accurate outcomes with fewer elements. This type of element allows the model to be simplified enough to be entirely meshed with cubic elements, improving mesh quality and reducing distortion. This is particularly useful in complex geometries, where hexahedral elements help maintain the precision and stability of the simulation results [37].

3. Mesh Convergence Analysis for Different Loading Protocols

3.1. Stress Fields and Estimated Fractional Errors

The mesh convergence analysis is based on the element quantity in the damper thickness. For each mesh size and number of cycles, the contour plot of the equivalent stress is shown. With the reduction in the size of the elements, the fields of stress, represented by colors, clearly differ in the areas where the maximum equivalent stress is produced (Figure 3). This localized zone is also important when studying the convergence of numerical results, as the gradient should be accurately reproduced and the variation in the results should be minimized when refinement is performed. The maximum stresses between the last two fine-mesh simulations are approximately the same. Note that the number of cycles does not create a significant difference in the stress fields, which is expected since the material is characterized by low strain hardening.

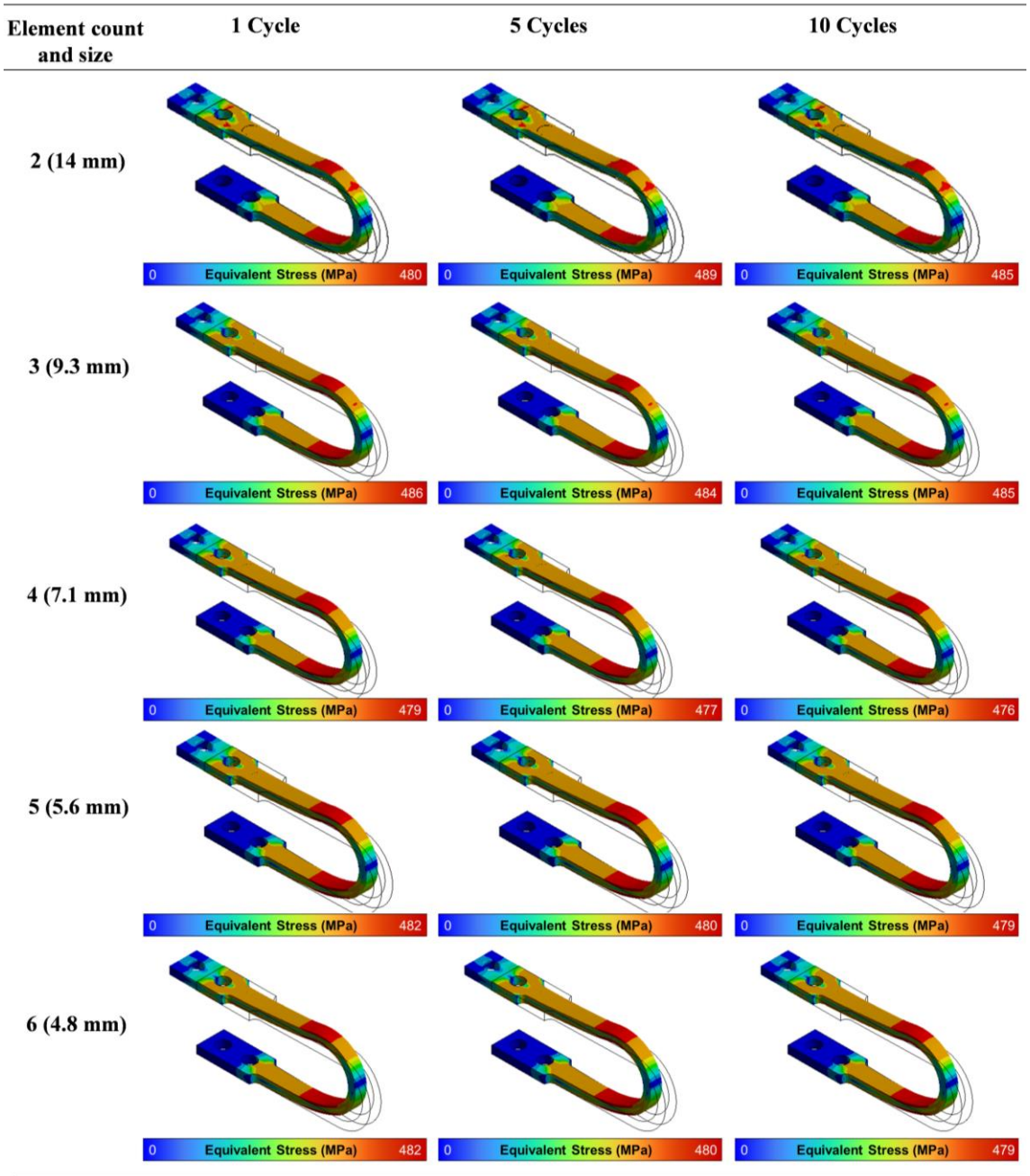

Figure 3. Maximum equivalent von Mises stress for the different mesh sizes in convergence analysis.

The trends of the fractional errors in the simulation results of the damper response at maximum stress levels for different loading protocols as a function of the element size are shown in Figure 4a through Figure 4c. According to the adapted Richardson extrapolation shown by the red curve, the increase in the fractional error stagnates at an element size of 5.6 mm (four elements in thickness). This is validated with the results from six elements.

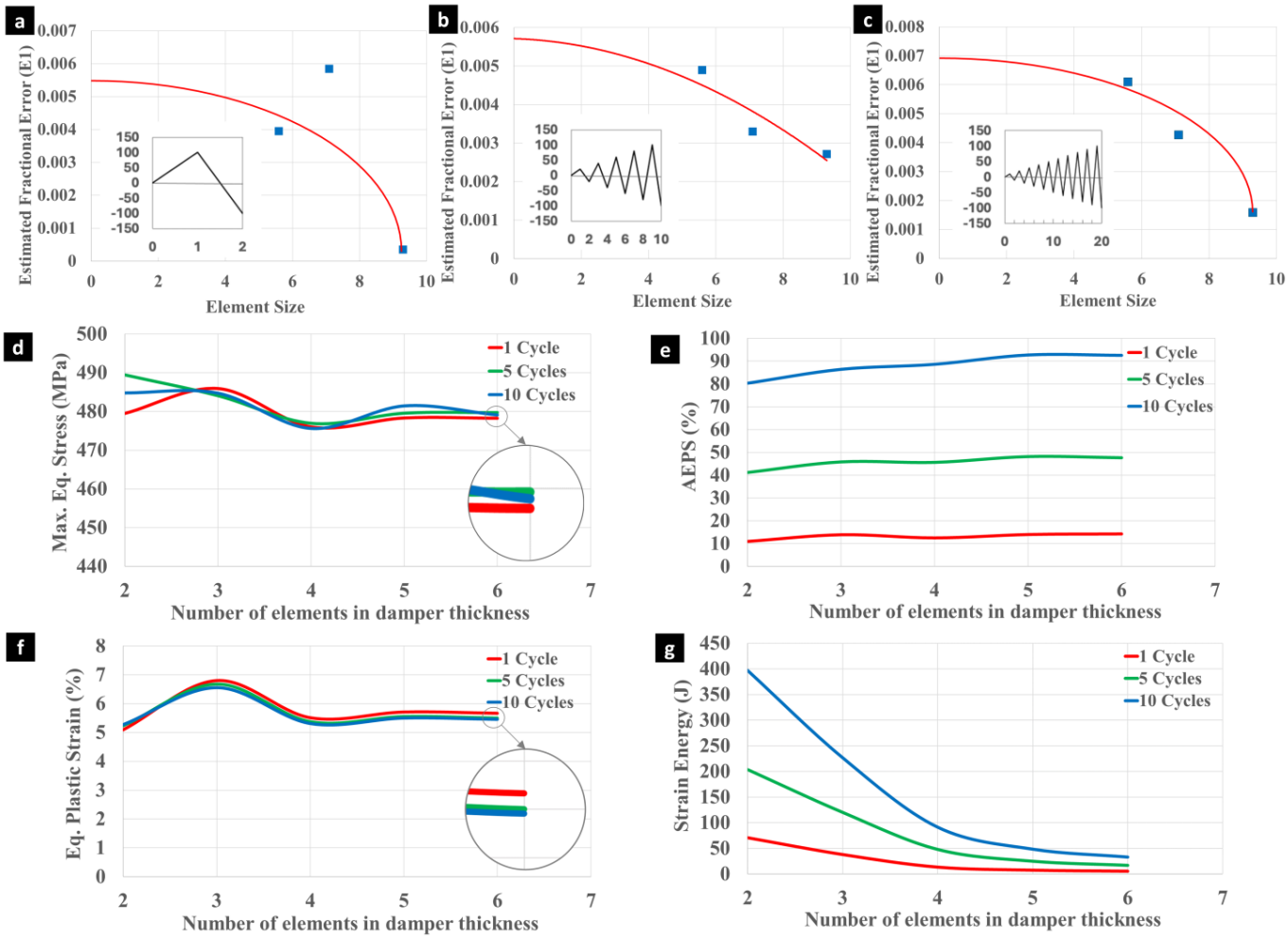

Figure 4. Mesh convergence analysis of (**a**) estimated fractional error (E1) vs. element size for 1 cycle, (**b**) 5 cycles, and (**c**) 10 cycles. (**d**) Maximum equivalent stress, (**e**) AEPS, (**f**) equivalent plastic strain, and (**g**) strain energy vs. number of elements in the damper thickness.

The maximum stress levels with an increasing number of elements per thickness are given in Figure 4d. The curve shows "wave-like" behavior until reaching an element size of 4.8 mm. The difference in the resulting maximum stress between 4.8 mm and 5.6 mm is negligible. When comparing these results with previous research, similar locations of maximum values of stress and strain are found in the damper; however, there is a notable difference in the through-thickness local behavior. This difference is due to the different number of elements included in the analysis. For example, Farajiani et al. [24] identified maximum stress values at similar locations of the dampers, but there was no variation in stress along the damper thickness. Zhang et al. [27] compared the equivalent plastic strain contours of different dampers, using three elements in the thickness of one damper and two in others. The resulting differences were attributed solely to the shape factors of the dampers, without taking into account the impact of the number of elements through the thickness of the damper, as given in Figures 3 and 4.

3.2. Impact of Mesh Size on Local Strain and Energy

The convergence results of the AEPS initially show a large distance between the curves due to the cumulative nature of this parameter. However, all three curves exhibit similar convergence trends, with the AEPS increasing until reaching a stagnation at the 4.8 mm mesh size. For the energy absorbed by the strain, a logarithmic behavior is observed, starting with significantly high values for larger element sizes and converging at less than 5 J. Additionally, a separation in the curves is observed because the number of cycles directly affects the amount of energy during the simulated loading protocols. These results show that the number of cycles is not an influential factor in the stress levels produced in the damper. However, the number of applied cycles influences the deformability and energy dissipation, considering the same level of maximum displacement.

A considerable difference in results was obtained between the 14 mm mesh size and 5.6 mm mesh size in terms of the equivalent plastic strain and the associated strain energy, indicating that to achieve good numerical results in U-shaped metallic dampers, the number of elements and size should not be selected randomly. In Atasever et al. [26], four elements in the damper thickness adequately captures the stress distribution, confirming our results; however, the low number of elements induces errors close to 10% in the equivalent plastic strain and lower accuracy for strain energy absorption compared to results with six elements per thickness, according to the convergence results reported in Figure 4f,g. In Qu et al. [38], the deviations between experimental and finite element modeling results still exist, possibly due to the low number of elements in the damper thickness (only two) and the consequent lack of accuracy in the local strain distribution compared to our numerical results. Similar analysis for the 14% higher damper stiffness and 9.4% of lower dissipated energy determined with one element in thickness were obtained in Jamkhaneh et al. [15].

This analysis demonstrated that mesh size significantly impacts stress and strain distribution in U-shaped dampers, influencing both the computation of strain energy and performance characteristics. Considering this convergence analysis and mesh refinement, a suitable grid for determining the behavior performance of the investigated U-shaped metallic damper via finite element-based computational analysis was established with a 4.8 mm element size, comprising six elements in thickness.

4. Simulation Results of Damper Behavior

The UD-40 model, meshed with a 4.8 mm element size, is subjected to a 20-step load protocol, allowing observation of its hysteretic behavior.

4.1. Local Phenomena: Strain, Stress, and Strain Energy

The computational results of stress fields, considering the maximum displacement applied in the load protocol, identify the highest stress levels between the curved and arms zones of the damper (Figure 5a). These results indicate that the head of the damper, where the bores are located, despite displaying mid-to-high stress levels, does not significantly impact the geometry, as it remains within its elastic zone. Figure 5b shows that the AEPS of the damper, with a maximum value of 93%, is also concentrated in a very localized part of the damper between the curve and the arms parts. The maximum equivalent stress of 476 MPa is lower than the ultimate tensile stress of the material, which is correlated with the maximum strain value of 5.5% (Figure 5c). When analyzing the reference bilinear curve of effective stress–strain values, the von Mises equivalent values shown in Figure 5a are coincident with the local strain values of Figure 5c. Additionally, the strain energy fields depicted in Figure 5d show the maximum values located in very small zones where the maximum stresses occur. This behavior is confirmed by other research, with maximum localized deformation in the damping section [15,26,38], while the trends in the through-thickness have only been found in [26].

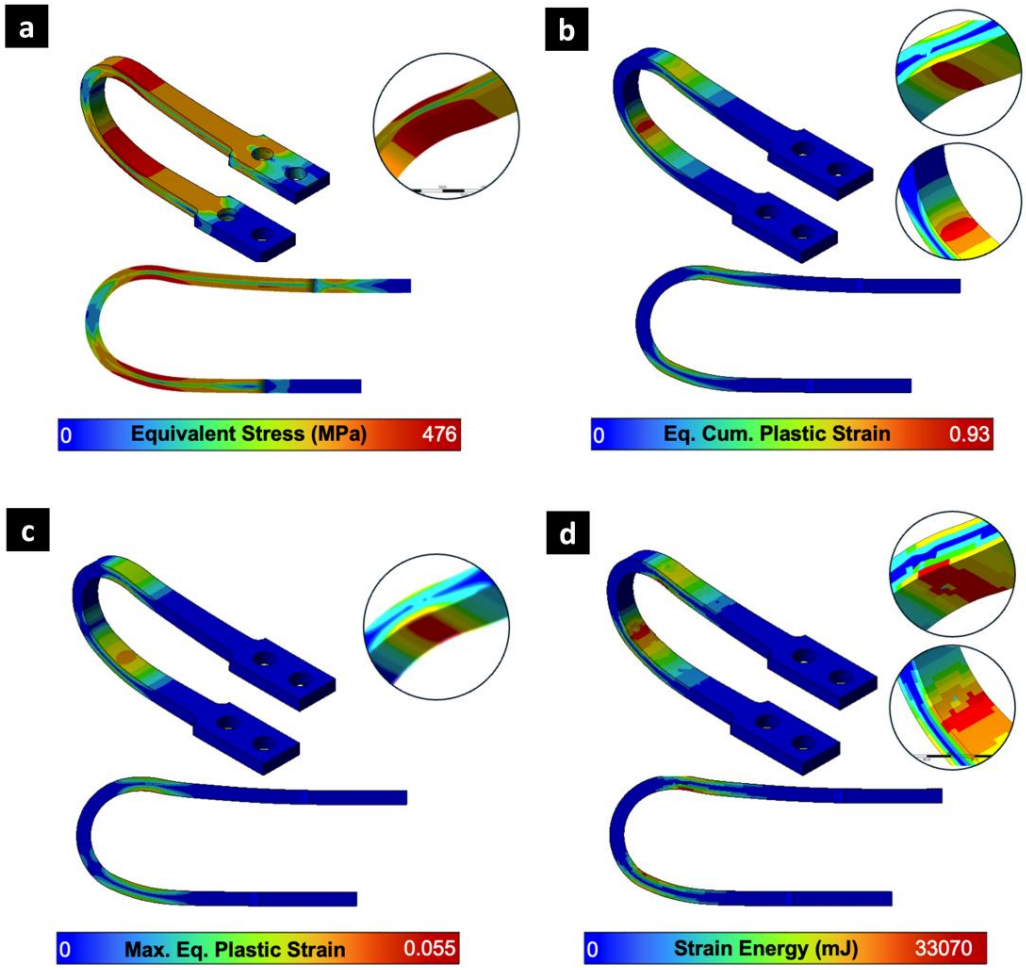

Figure 5. Fields of (**a**) equivalent von Mises stress, (**b**) equivalent cumulative plastic strain (AEPS), (**c**) equivalent plastic strain, and (**d**) strain energy on the ultimate applied displacement.

A summary of the results of the local maximum values of the von Mises equivalent stress, strain, and energy for the maximum displacement of the 20-step load protocol is shown in Table 3. The maximum stress level is adequately located between the initial yield stress and the ultimate strength, confirming that the damper is working in the ductile plastic zone. This plastic deformation allows the device to dissipate energy transferred from the corresponding structure. Note that the AEPS is considerably greater than the equivalent strain because of the 20-step load; this is expected, as in each cycle, the AEPS increases with monotonic plastic strain. The strain energy shown in Figure 5d indicates the energy absorbed by the dampers, which is not stored after the recovery of elastic strain.

Table 3. Summary of simulation results of damper behavior at the ultimate applied displacement.

Equivalent Stress (MPa)	AEPS	Equivalent Strain	Strain Energy (mJ)	Energy per Unit Volume (mJ/mm^3)	Dissipated Energy (mJ)
475.2	0.925	0.055	33,070	22.7	51,166

4.2. Overall Performance: Stiffness, Reaction Forces, and Energy Dissipation Capacity

Reaction forces, energy dissipation, stiffness properties, and overall performance under cyclic loading conditions are computed from the hysteresis curve (Figure 6a). This curve compares the reaction forces at the lower bolts against the applied displacements. The bilinear behavior assigned to the material reveals a nonlinear model prediction when the loop is examined. This is attributed to the inhomogeneity of local stress behavior;

while some parts are under elasticity, localized zones reach plasticity, converting the overall performance to nonlinear. The symmetrical skeleton curve from the force peaks at the end of each load step is attributed to isotropic hardening. The predicted increasing peak force at the end of each cycle is due to the hardening behavior that alters the yield limit of the material with each load. To validate the numerical model, the hysteresis curve is compared in Figure 6a with experimental data from Suzuki et al. [19]. Their experiments involved testing UD-40 damper specimens with similar dimensions, fabricated from JIS SM490 steel, under horizontal cyclic loading. The specimens were fixed at their upper and lower ends to a horizontal axial machine using bolted connections. A 500-kN actuator applied sinusoidal displacement-controlled loading at an average speed of 10 mm/s and amplitudes of 10, 30, 50, and 100 mm. Displacement measurements were acquired using wire displacement transducers located in the upper supporting beam, while load measurements were obtained using a built-in load cell located below the lower plate.

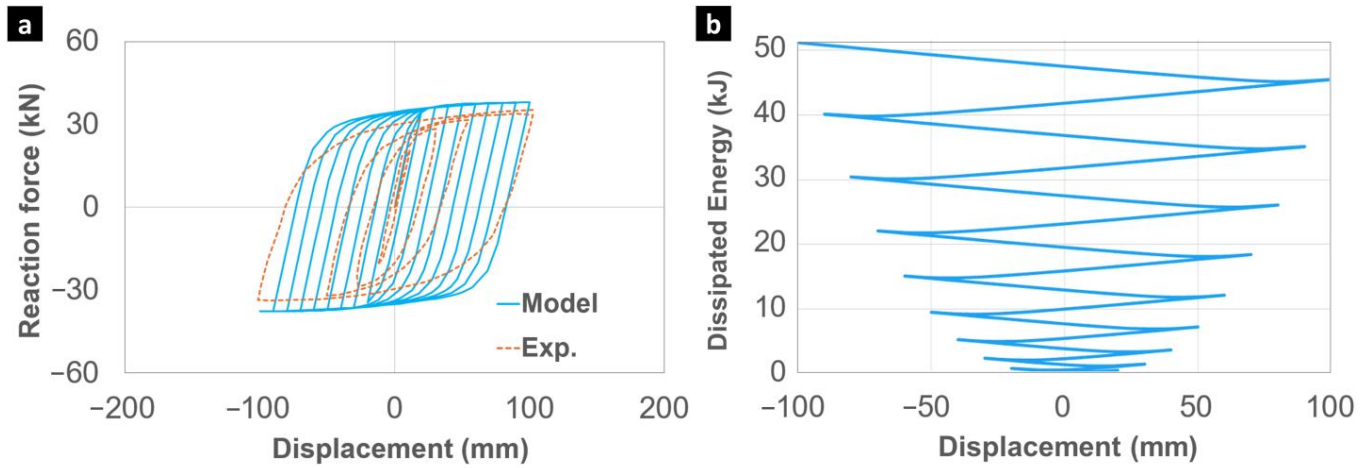

Figure 6. (**a**) Hysteresis curve and (**b**) plastic strain energy vs. displacement.

The computational model predicts higher reaction force values within the investigated displacement range, which is a direct result of the bilinear approximation of the hardening behavior. Figure 1 shows clearly that the higher slope of the bilinear model compared to the true stress–strain curve affects the estimated stress levels in the damper. This overestimation of strain hardening is most evident in the prediction of yield strength from initial yielding up to 3% strain. The discrepancy in hardening is identified as the primary source of error, given that the damper primarily experiences local strains ranging from 0 to 5.5%. However, the average relative error of the model in the stress values is only 7.8%, which falls within an acceptable range for validating the effectiveness of the computational model in predicting the performance of the UD-40 damper.

A key feature of this hysteresis curve is that the area within the loop directly represents the energy dissipated by the damper as plastic work. The stiffness levels are calculated via Equation (7). The stiffness is divided into two types: the first stiffness or elastic stiffness produced in the elastic zone, and the second stiffness or postelastic stiffness produced in the plastic zone. Both are calculated via Equation (7), as proposed by Nguyen and Guizani [39].

$$k_e = \frac{1}{\frac{2LR^2}{EI_{y1}} + \frac{\pi R^3}{2EI_{y2}}} \tag{7}$$

$$I_{y1} = \frac{w_1 t^3}{12} \tag{8}$$

$$I_{y2} = \frac{w_2 t^3}{12} \tag{9}$$

In Equation (7), k_e is the first stiffness. L is the arm's length of the damper; R is the radius of the curve; and E is the Young's modulus. I_{y1} and I_{y2} represent the stiffness to bending for the arms and curve of the damper, respectively. Specifically, in Equation (8), w_1 is the average width of the arms, and for Equation (9), w_2 is the average width of the curve section of the damper. For both, t is the thickness.

Although the second stiffness exhibited during the nonlinear behavior of the damper cannot be deduced from a simple analytical expression, experimental observations suggest that it may approximate 0.1 to 0.5 times the initial stiffness [39]. For the purposes of this paper, the second stiffness is assumed to be 0.1 times the initial stiffness.

Additionally, an analytical comparison between the stiffnesses of each damper is performed using the basics of springs from Equations (10) and (11) [40]. These equations do not consider the geometrical data of the damper, but only the reaction forces (F) and the displacement (δ). The analysis will be performed in the first step, using a maximum displacement of 10 mm.

$$k_e = \frac{F}{\delta} \tag{10}$$

$$k_p = \frac{\Delta F}{\Delta \delta} \tag{11}$$

where k_p is the second stiffness, ΔF is the difference in the forces applied in the plastic zone of the curve, and $\Delta\delta$ is the difference between the displacements in the same zone. The load protocol for the analysis considers 20 steps from 0 to $\pm$100 mm applied to the upper bores. Table 4 shows the comparison between the stiffness given by the geometrical parameters (GS) and that by the reaction/displacement parameters (RDS). The experimental first stiffness reported in Suzuki et al. [19] is included, while the second stiffness is computed from the reported experimental hysteresis curve in similar displacement intervals.

Table 4. Stiffness obtained via the GS and RDS methods compared to experimental data.

	Stiffness (N/mm)		**Relative Error (%)**		
	1st	**2nd**	**1st**	**2nd**	**Global**
Experimental [19]	2000	100			
GS [39]	1920	192	4	96	46
RDS	2308	82	15	16	16

Table 4 demonstrates a notable difference between the two methods, with the RDS method yielding higher values for the first stiffness compared to the GS method. This difference can be attributed to the conditions of the study, where the RDS method considers both the geometrical and boundary conditions, against the GS, which only depends on the geometry of the damper. The second stiffness with RDS methods provides values closer to experimental data than GS. This is related to the nonlinearity of plastic behavior in the damper, with local values reaching plasticity while others behave elastically, a phenomenon that cannot be described by the GS method. Compared to experimental results reported in ref. [19], GS yields accurate prediction of stiffness with a 16% relative error compared to the RDS method with a 46% global relative error. These discrepancies could be affected by the accuracy of experimental data, error bars, intervals of considered displacements, and the non-reported method selected by the authors to compute the experimental stiffness [19].

Figure 6b shows the increase in energy dissipated by the damper with the applied displacement. The vertical distance between the peaks at each displacement is increasing with each cycle, indicating that the energy dissipated grows exponentially. In the model damper, under ten cycles, the maximum dissipated energy reaches 50 kJ. The number of cycles and the energy that the damper can dissipate are ongoing research topics that involve calibrating appropriate damage-fatigue models.

5. Future Research

5.1. Optimizing Seismic Response and Lifetime of U-Shaped Dampers

The detailed numerical models that characterize local stress, strain, and energy dissipation patterns provide a solid foundation for optimizing the design of high-performance U-shaped dampers for seismic applications. Various optimization approaches could be explored, such as maximizing the energy dissipation capacity, bidirectional capability, optimizing material selection, and achieving a more homogeneous strain distribution to enhance fatigue life. Furthermore, the integration of the design of experiment methodologies could reduce the number of numerical models required during the optimization process. Additionally, the reliable mesh discretization established by this numerical model enables the application of more sophisticated models that consider micromechanical damage, fracture prediction, and fatigue behavior, ultimately leading to accurate lifetime predictions for U-shaped dampers and, consequently, safer designs to improve structural resilience during seismic events.

5.2. Toward Simplified Model of U-Shaped Damper Hysteresis

This study provides a foundation for developing a simplified model performance of the U-shaped damper. A simplified force–displacement relationship model should be easily incorporated into larger structural models, thereby reducing computational demands but without compromising accuracy. This future research can benefit from exploring the simplified models discussed by Wang and Mahin [41] and Zhai et al. [42], and their significance in the context of seismic applications. To express the hysteretic behavior using parametric equations involving the key geometric parameters, such as height, thickness, and width of the U-shaped damper, the validated numerical tool should be used. The obtained approach is expected to enable other researchers to easily adapt the damper configurations for diverse application requirements, including large-scale building structures, without the need for complex and computationally intensive numerical simulations.

5.3. Re-Centering Limitations of U-Shaped Dampers

Although the proposed U-shaped damper offers several advantages, including high energy dissipation capacity, large deformation ability, a simple design, ease of fabrication and installation, cost-effectiveness, and adaptability to various structural applications, it is crucial to acknowledge its inherent limitation regarding re-centering capability. In contrast to self-centering systems, conventional U-shaped dampers display residual deformation following cyclic loading, which may have an adverse effect on structural performance during subsequent seismic events. Such residual deformation can accumulate over multiple cycles, which may result in increased interstory drifts and potential damage. It is therefore vital to address this limitation in order to guarantee the long-term seismic resilience of structures that employ these dampers. Strategies such as incorporating pre-tensioned tendons or shape memory alloys, as demonstrated in self-centering dissipative braces [43,44], present potential solutions for mitigating residual deformations and enhancing the re-centering capability. These systems derive their functionality from the elastic energy stored in pre-tensioned elements, which is employed to restore the structure to its original position after an earthquake. Promising future research involves the development of hybrid systems that combine the energy dissipation capabilities of U-shaped dampers with the re-centering properties of these self-centering mechanisms. Such hybrid systems have the potential to significantly enhance the performance and broaden the applicability of U-shaped dampers in earthquake-resistant design.

6. Conclusions

This work advanced the design of U-shaped (USSD) dampers through the development and validation of a computational model for detailed analysis of the local phenomena of stress, strain, and energy dissipation. The key findings are as follows:

- Adapting the Richardson method for mesh convergence analysis proves effective for solid mechanics problems, particularly seismic damper modeling. While Richardson extrapolation is frequently used in computational fluid dynamics, this adaptation offers a robust and efficient method to determine reliable mesh densities for accurately simulating seismic damper behavior.
- For reliable numerical simulation results of local strain and energy, at least four elements' through-thickness is required in U-shaped dampers. The influence of mesh density on simulation accuracy is less sensitive to maximum local stress than the maximum strain.
- Distinct zones of high stress gradients within the damper highlight the coexistence of elastic and localized plastic deformation mechanisms. Elastic regions, primarily contributing to energy storage, and the localized plastic zones responsible for the critical energy dissipation through plastic work demonstrate the potential for damper optimization.
- The highest equivalent stresses are at the transitions between flat and curved sections, with local stresses below the ultimate strength confirming adequate nonlinear computation.
- The geometry based GS approach proved highly inaccurate for computing the second stiffness compared to the RDS method (primarily due to its focus on geometry), while the RDS method incorporates essential aspects such as material nonlinearity.

The proposed computational model demonstrated reliable elastoplastic numerical results for the performance response of U-shaped seismic dampers. This tool should be applied to optimize current designs and to develop new performance-efficient USSDs. The incorporation of a more sophisticated fatigue-damage model should provide the required simulation results for ensuring the damper lifespan and reliability of buildings and structures in seismic regions. Future research should also focus on three key areas: developing simplified, computationally efficient models of U-shaped damper behavior suitable for integration into larger structural analyses; exploring hybrid systems that combine the energy dissipation of U-shaped dampers with the re-centering capabilities of other mechanisms like pre-tensioned tendons or shape memory alloys to mitigate residual deformation; and conducting parametric studies to express the hysteretic behavior of these dampers using key geometric parameters, facilitating the rapid selection process of seismic dampers for diverse applications without complex numerical simulations.

Author Contributions: Á.G.: Investigation, formal analysis, writing—original draft; visualization; data curation; V.T.: conceptualization, methodology, investigation; formal analysis, writing—original draft, writing—review and editing, supervision, project administration; F.B.: writing—review and editing, formal analysis; A.O.: writing—review and editing, formal analysis; J.H.: writing—review and editing, formal analysis; C.G.: software; L.D.: writing—review and editing, supervision; A.-M.H.: writing—review and editing, resources. All authors have read and agreed to the published version of the manuscript.

Funding: This research was partially funded by the WBI/AGCID RI02 (DIE23-0001) bilateral project between the University of Liège and the Universidad de La Frontera. F. Bustos thanks the Agencia Nacional de Investigación y Desarrollo (ANID) for the Ph.D. scholarship "Beca Doctorado Nacional/2020-21200973".

Institutional Review Board Statement: Not applicable.

Informed Consent Statement: Not applicable.

Data Availability Statement: The original contributions presented in the study are included in the article; further inquiries can be directed to the corresponding author.

Conflicts of Interest: The authors declare that they have no known competing financial interests or personal relationships that could have appeared to influence the work reported in this paper.

References

1. MOP; MinInterior; MinHacienda; MIDEPLAN; SEGPRES. Plan de Reconstrucción Terremoto y Maremoto del 27 de Febrero de 2010 Resumen Ejecutivo. 2010. Available online: https://www.desarrollosocialyfamilia.gob.cl/pdf/plan-reconstruccion-resumen-ejecutivo.pdf (accessed on 22 August 2023).
2. Daniell, J.E.; Wenzel, F. A Timeline of the Socio-Economic Effects of the 2011 Tohoku Earthquake with Emphasis on the Development of a New Worldwide Rapid Earthquake Loss Estimation Procedure HARIS-SCM. Available online: https://www.researchgate.net/publication/258434194 (accessed on 22 August 2023).
3. Bustos, F.; Hinojosa, J.; Tuninetti, V. Computational Comparison of Performance of Different Steel Plate Shear Yielding Dampers. *Buildings* **2023**, *13*, 793. [CrossRef]
4. Javanmardi, A.; Ibrahim, Z.; Ghaedi, K.; Benisi Ghadim, H.; Hanif, M.U. State-of-the-Art Review of Metallic Dampers: Testing, Development and Implementation. *Arch. Comput. Methods Eng.* **2020**, *27*, 455–478. [CrossRef]
5. Li, S.; Jia, Z.; Ye, Q. Study on Dynamic Response of Damper under Gas Explosion Impact. *Sustainability* **2023**, *15*, 3356. [CrossRef]
6. Liang, L.; Feng, Z.; Xu, Y.; Chen, Z.; Liang, L. A Parallel Scheme of Friction Dampers and Viscous Dampers for Girder-End Longitudinal Displacement Control of a Long-Span Suspension Bridge under Operational and Seismic Conditions. *Buildings* **2023**, *13*, 412. [CrossRef]
7. Pecora, R. A Practical Approach for the Mitigation of Seismic-Induced Vibrations in Slender Metallic Structures through Magnetorheological Fluid Dampers. *Appl. Sci.* **2022**, *12*, 4155. [CrossRef]
8. You, J.; Yang, Y.; Fan, Y.; Zhang, X. Seismic Response Study of L-Shaped Frame Structure with Magnetorheological Dampers. *Appl. Sci.* **2022**, *12*, 5976. [CrossRef]
9. Xu, G.; Ou, J. Seismic performance of combined rotational friction and flexural yielding metallic dampers. *J. Build. Eng.* **2022**, *49*, 104059. [CrossRef]
10. Mou, B.; Wang, Z.; Zhang, Z.; Wu, C. Seismic behavior of steel frames with H-shaped damper. *J. Constr. Steel Res.* **2024**, *213*, 108401. [CrossRef]
11. Kim, Y.-C.; Mortazavi, S.J.; Farzampour, A.; Hu, J.-W.; Mansouri, I.; Awoyera, P.O. Optimization of the Curved Metal Damper to Improve Structural Energy Dissipation Capacity. *Buildings* **2022**, *12*, 67. [CrossRef]
12. Zlatkov, D.; Ristić, D.; Zorić, A.; Ristić, J.; Mladenović, B.; Petrović, Ž.; Trajković-Milenković, M. Experimental and Numerical Study of Energy Dissipation Components of a New Metallic Damper Device. *J. Vib. Eng. Technol.* **2022**, *10*, 1809–1829. [CrossRef]
13. Al-Sadoon, Z.A.; Leblouba, M.; Fageeri, A. Experimental validation of a novel curved steel damper for steel frames with flexible beam-column joints. *Structures* **2023**, *56*, 105010. [CrossRef]
14. Kelly, J.M.; Skinner, R.I.; Heine, A.J. Mechanisms of energy absorption in special devices for use in earthquake resistant structures. *Bull. N. Z. Soc. Earthq. Eng.* **1972**, *5*, 63–88. [CrossRef]
15. Ebadi Jamkhaneh, M.; Ebrahimi, A.H.; Shokri Amiri, M. Experimental and Numerical Investigation of Steel Moment Resisting Frame with U-Shaped Metallic Yielding Damper. *Int. J. Steel Struct.* **2019**, *19*, 806–818. [CrossRef]
16. Qiu, C.X.; Huang, T.Y.; Wang, Y.Z.; Qian, H.J. Theoretical and experimental study on seismic performance of T-section metallic damper. *J. Constr. Steel Res.* **2023**, *211*, 108161. [CrossRef]
17. Ene, D.; Kishiki, S.; Yamada, S.; Jiao, Y.; Konishi, Y.; Terashima, M.; Kawamura, N. Experimental study on the bidirectional inelastic deformation capacity of U-shaped steel dampers for seismic isolated buildings. *Earthq. Eng. Struct. Dyn.* **2016**, *45*, 173–192. [CrossRef]
18. Khatibinia, M.; Jalaipour, M.; Gharehbaghi, S. Shape optimization of U-shaped steel dampers subjected to cyclic loading using an efficient hybrid approach. *Eng. Struct.* **2019**, *197*, 108874. [CrossRef]
19. Suzuki, K.; Watanabe, A.; Saeki, E. Development of U-Shaped Steel Damper for Seismic Isolation System. 2005. Available online: https://www.nipponsteel.com/en/tech/report/nsc/no92.html (accessed on 16 May 2024).
20. Satria, E.; Son, L.; Bur, M.; Akbar, M.; Haris, S. Numerical analysis of U-shaped hysteresis steel damper with energy absorber for seismic areas. *IOP Publ.* **2019**, *602*, 012078. [CrossRef]
21. Greco, A.; Fiore, I.; Occhipinti, G.; Caddemi, S.; Spina, D.; Caliò, I. An Equivalent Non-Uniform Beam-Like Model for Dynamic Analysis of Multi-Storey Irregular Buildings. *Appl. Sci.* **2020**, *10*, 3212. [CrossRef]
22. Kim, S.-W.; Kim, K.-H. Evaluation of Structural Behavior of Hysteretic Steel Dampers under Cyclic Loading. *Appl. Sci.* **2020**, *10*, 8264. [CrossRef]
23. Liu, Y.; Ikeda, S.; Liu, Y.; Kang, L.; Ge, H. Experimental Investigation of Fracture Performances of SBHS500, SM570 and SM490 Steel Specimens with Notches. *Metals* **2022**, *12*, 672. [CrossRef]
24. Farajiani, F.; Elyasigorji, F.; Elyasigorji, S.; Moradi, M.J.; Farhangi, V. Effect of U-Shaped Metallic Dampers on the Seismic Performance of Steel Structures based on Endurance-Time Analysis. *Buildings* **2024**, *14*, 1368. [CrossRef]
25. NSE. Response Control and Seismic Isolation Devices. 2024. Available online: https://www.eng.nipponsteel.com/en/business/building_and_infrastructure/ (accessed on 25 October 2024).
26. Atasever, K.; Celik, O.C.; Yuksel, E. Development and Cyclic Behavior of U-Shaped Steel Dampers with Perforated and Nonparallel Arm Configurations. *Int. J. Steel Struct.* **2018**, *18*, 1741–1753. [CrossRef]
27. Zhang, Z.X.; Zhang, J.; Fang, C.; Zhang, Y.; Li, Y. Emerging steel frames with Fe-SMA U-shaped dampers for enhancing seismic resilience. *J. Infrastruct. Preserv. Resil.* **2023**, *4*, 6. [CrossRef]

28. Bagheri, S.; Barghian, M.; Saieri, F.; Farzinfar, A. U-shaped metallic-yielding damper in building structures: Seismic behavior and comparison with a friction damper. *Structures* **2015**, *3*, 163–171. [CrossRef]
29. Kishiki, S.; Zheng, H.; Ishida, T.; Tatsumi, N.; Watanabe, A. Inspection of U-shaped steel dampers based on residual plastic deformation. *Eng. Struct.* **2021**, *245*, 112915. [CrossRef]
30. PNS ASTech. Vibration Control and Seismic Isolation Devices. Available online: https://www.pnsastech.com.ph/Response-Control-Seismic-Isolation-Devices.php (accessed on 26 October 2024).
31. Efinger, D.; Ostertag, A.; Dazer, M.; Borschewski, D.; Albrecht, S.; Bertsche, B. Reliability as a Key Driver for a Sustainable Design of Adaptive Load-Bearing Structures. *Sustainability* **2022**, *14*, 895. [CrossRef]
32. Nateghi, F.A.; Torbat, M.E. Improved Behaviour of Accordion Metallic Dampers Affected by the Increasing Number of Layers. *Int. J. Eng.* **2015**, *28*, 864–870.
33. Tuninetti, V.; Mariqueo, M. Performance of Combined Woven Roving and Mat Glass-Fiber Reinforced Polymer Composites Under Absorption Tower Lifting Loads. *Polymers* **2024**, *16*, 2937. [CrossRef]
34. Hosford, W.F.; Caddell, R.M. *Metal Forming: Mechanics and Metallurgy*; Cambridge University Press: Cambridge, UK, 2011. Available online: https://books.google.cl/books/about/Metal_Forming.html?id=x0GWAd7hNy0C&redir_esc=y (accessed on 13 May 2024).
35. Szybiński, B.; Romanowicz, P.J. Optimization of Flat Ends in Pressure Vessels. *Materials* **2019**, *12*, 4194. [CrossRef]
36. Slater, J.W. Examining Spatial (Grid) Convergence. Available online: https://www.grc.nasa.gov/www/wind/valid/tutorial/spatconv.html (accessed on 14 May 2024).
37. Ferris, T. 3 Steps to Improve FEA Models. Available online: https://www.ansys.com/blog/how-to-improve-fea (accessed on 26 May 2024).
38. Qu, C.-X.; Xu, Y.-W.; Gao, J.-H.; Zhou, W.-H.; Zheng, B.-Z.; Li, P. Mechanical Performance Study of Beam–Column Connection with U-Shaped Steel Damper. *Materials* **2022**, *15*, 7085. [CrossRef]
39. Nguyen, X.D.; Guizani, L. Analytical and numerical investigation of natural rubber bearings incorporating U-shaped dampers behaviour for seismic isolation. *Eng. Struct.* **2021**, *243*, 112647. [CrossRef]
40. Beer, F.P.; Johnston, E.R.; DeWolf, J.; Mazurek, D.F. *Mechanics of Materials*, 8th ed.; McGraw-Hill: New York, NY, USA, 2019.
41. Wang, S.; Mahin, S.A. High-performance computer-aided optimization of viscous dampers for improving the seismic performance of a tall building. *Soil Dyn. Earthq. Eng.* **2018**, *113*, 454–461. [CrossRef]
42. Zhai, Z.; Guo, W.; Yu, Z.; He, C.; Zeng, Z. Experimental and numerical study of S-shaped steel plate damper for seismic resilient application. *Eng. Struct.* **2020**, *221*, 111006. [CrossRef]
43. Yan, X.; Shu, G.; Rahgozar, N.; Alam, M.S. Seismic design and performance evaluation of hybrid braced frames having buckling-restrained braces and self-centering viscous energy-dissipative braces. *J. Constr. Steel Res.* **2024**, *213*, 108359. [CrossRef]
44. De Domenico, D.; Gandelli, E.; Gioitta, A. Displacement-based design procedure for the seismic retrofit of existing buildings with self-centering dissipative braces. *Structures* **2024**, *62*, 106174. [CrossRef]